nature nanotechnology

ARTICLES

PUBLISHED ONLINE: 22 JUNE 2015 | DOI: 10.1038/NNANO.2015.130

A pH-independent DNA nanodevice for quantifying chloride transport in organelles of living cells

Sonali Saha[1], Ved Prakash[2], Saheli Halder[1], Kasturi Chakraborty[2] and Yamuna Krishnan[1,2]*

The concentration of chloride ions in the cytoplasm and subcellular organelles of living cells spans a wide range (5–130 mM), and is tightly regulated by intracellular chloride channels or transporters. Chloride-sensitive protein reporters have been used to study the role of these chloride regulators, but they are limited to a small range of chloride concentrations and are pH-sensitive. Here, we show that a DNA nanodevice can precisely measure the activity and location of subcellular chloride channels and transporters in living cells in a pH-independent manner. The DNA nanodevice, called Clensor, is composed of sensing, normalizing and targeting modules, and is designed to localize within organelles along the endolysosomal pathway. It allows fluorescent, ratiometric sensing of chloride ions across the entire physiological regime. We used Clensor to quantitate the resting chloride concentration in the lumen of acidic organelles in *Drosophila melanogaster*. We showed that lumenal lysosomal chloride, which is implicated in various lysosomal storage diseases, is regulated by the intracellular chloride transporter DmClC-b.

Lumenal chloride is critical to organelle function and is regulated by intracellular chloride transporters such as Cl^-/H^+ exchangers or chloride channels[1–3]. The small size of organelles and the difficulty in obtaining contamination-free intracellular membranes has made the study of subcellular chloride and its regulators technically challenging to address by electrophysiology. An alternative route to address the activity of a given intracellular chloride regulator of interest would be to quantify resting lumenal chloride within the relevant subcellular organelle. Chloride-sensitive protein reporters do exist, such as Clomelon[4], Cl-Sensor[5] and ClopHensor[6]. However, most are valid only over a limited range of chloride and are pH-sensitive. Subcellular organelles span a wide range of pH. For example, lysosomal pH is close to 5.0, the trans-Golgi network has a pH of 6.0, and the endoplasmic reticulum has a pH of 7.2[7]. Moreover, chloride accumulation is frequently coupled to lumenal acidity and so pH-dependent chloride reporters cannot be used to assay intracellular chloride regulators[8]. ClopHensor—a possible exception—is a chloride reporter with a built-in pH reporter, whereby chloride may be estimated using relatively complex pH correction factors. However, because it is a binding-based sensor, it is not applicable to all physiological chloride concentrations[6]. Chloride-sensitive small-molecule dyes such as 6-methoxy-*N*-(3-sulphopropyl) quinolinium (SPQ)[9], 6-methoxy-quinolyl acetoethyl ester (MQAE)[10] and lucigenin[11] are other possibilities. They are pH-insensitive, function by collisional quenching, and are therefore uniformly sensitive to chloride across the entire physiological regime[12]. However, these dyes cannot be specifically localized within organelles. Attempts to target these dyes to specific organelles by chemical conjugation to ligands or polymers lead to either massive fluorescence quenching and/or highly variable sensor characteristics, because the location and degree of functionalization on the polymer cannot be controlled[8,13]. There is therefore an unmet need for a fluorescent chloride sensor that (1) has uniform performance characteristics, (2) operates over the entire physiological range of $[Cl^-]$ and (3) is pH-independent so that it is able to quantify organellar chloride in living cells.

Nucleic acids are modular, targetable and programmable, and are therefore well-suited for the design of specific, sensitive and quantitative reporters for molecular inputs that can be transduced into fluorescent readouts[14,15]. With nucleic acids one can realize molecularly identical assemblies with negligible batch-to-batch variation[16–19]. This results in nanodevices with highly uniform reporter characteristics that are preserved across diverse cells and pathways, predisposing them to studies based on comparative assays. Molecularly identical sensors are critical for the study of inherent heterogeneities or spreads in resting analyte concentrations present in biological systems of different genetic backgrounds. We have realized nucleic-acid-based nanodevices that precisely report the pH associated with endosomal maturation[16,20] and address their crosstalk with the secretory pathway[17]. These molecular devices can be coupled to simple organelle localization strategies that co-opt specific cellular trafficking pathways[17,21]. Here, we integrate these trafficking strategies to specifically localize a chloride-sensitive DNA-based nanodevice—called Clensor—within organelles along the endolysosomal pathway. We delineate a generalizable methodology to investigate the activity of intracellular chloride regulators in living cells using this pH-independent, fluorescent, ratiometric DNA-based chloride reporter. We demonstrate this by identifying the localization and function of the CLC family of proteins along the endolysosomal pathway in *Drosophila melanogaster*.

Design and *in vitro* characterization of Clensor

Clensor is composed of three modules: (1) sensing (P), (2) normalizing (D2) and (3) targeting (D1) modules (Fig. 1a). Sensing module P is a 12-mer peptide nucleic acid (PNA) sequence conjugated to a fluorescent, chloride-sensitive molecule 10,10′-bis[3-carboxypropyl]-9,9′-biacridinium dinitrate (BAC)[8]. Normalizing module D2 is a

[1]National Centre for Biological Sciences, TIFR, GKVK, Bellary Road, Bangalore 560065, India. [2]Department of Chemistry, University of Chicago, 929E, 57th Street, E305A, GCIS, Chicago, Illinois 60637, USA. *e-mail: yamuna@uchicago.edu

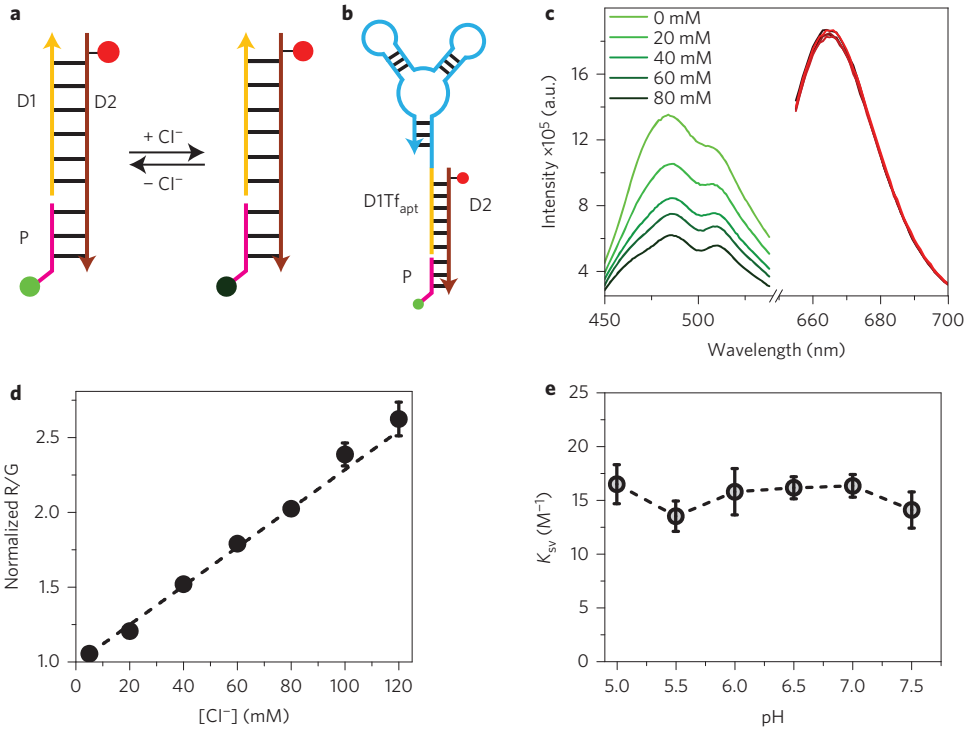

Figure 1 | Design and characterization of Clensor and Clensor^{Tf}. **a**, Structure and working principle of Clensor. P, sensing module (pink line) containing a Cl^--sensitive fluorophore, BAC (green filled circle); D2, normalizing module (brown line) containing a Cl^--insensitive fluorophore, Alexa 647 (red filled circle); D1, targeting module (orange line). In the presence of Cl^-, BAC undergoes collisional quenching, whereas fluorescence of Alexa 647 is Cl^--independent. **b**, Modified sensor design for targeting to the recycling pathway (Clensor^{Tf}). D1Tf$_{apt}$, targeting module modified with an RNA aptamer (Tf$_{apt}$) against the human transferrin receptor (cyan line). **c**, Fluorescence emission spectra of Clensor at the indicated [Cl^-] obtained using λ_{Ex}^{BAC} = 435 nm (green) and $\lambda_{Ex}^{Alexa\ 647}$ = 650 nm (red). **d**, *In vitro* Cl^- calibration profile of Clensor showing normalized Alexa 647 and BAC fluorescence intensity ratio (R/G) versus [Cl^-]. R/G values at different chloride concentrations were normalized to the value at 5 mM chloride. **e**, Plot of K_{SV} for Clensor versus pH. Error bars indicate the mean of three independent experiments ± s.e.m.

38-mer DNA sequence bearing an Alexa 647 fluorophore (A647) that is Cl^--insensitive. Targeting module D1 is a 26-mer DNA sequence. P and D1 are hybridized to adjacent sites on D2, as shown in Fig. 1a. The dsDNA domain on Clensor, comprising D1 and D2, functions as a negatively charged ligand for trafficking along the endolysosomal pathway mediated by anionic ligand binding receptors (ALBRs)[16]. To traffic Clensor along the transferrin pathway, we molecularly programmed the targeting module (D1) of Clensor by conjugating its 5′ terminus to a well-characterized RNA aptamer (Tf$_{apt}$) to the human transferrin receptor[22] to give a DNA–RNA chimeric oligonucleotide called D1Tf$_{apt}$ (Fig. 1b). The chloride sensor thus programmed to target the transferrin pathway consists of P, D2 and D1Tf$_{apt}$, and is called Clensor^{Tf}. The formation of Clensor and Clensor^{Tf} was confirmed by a gel shift assay (Supplementary Fig. 1).

BAC undergoes collisional quenching specific to Cl^- that is expected to reduce its fluorescence intensity, G, linearly with [Cl^-][8]. In contrast, the fluorescence intensity of A647, R, remains constant (Fig. 1c). This results in different ratios of the emission intensities (R/G) for A647 (λ_{Em} = 670 nm, R) and BAC (λ_{Em} = 505 nm, G) over physiological [Cl^-] (Fig. 1c,d). This ratiometric approach enables the quantitation of lumenal chloride, [Cl^-]$_{lumen}$, within endolysosomal compartments. The fluorescence properties of Clensor (200 nM) were investigated as a function of [Cl^-] to evaluate its Cl^- sensitivity. As expected, R is unaffected with increasing [Cl^-], while G decreases linearly (Fig. 1c). A plot of the normalized R/G values as a function of [Cl^-] yielded the *in vitro* Cl^- calibration profile for Clensor (Fig. 1d). We see that the Cl^- sensitivity of Clensor varies linearly with [Cl^-] up to at least 120 mM, with a apparent Stern–Volmer quenching constant K_{SV} of 12.9 M^{-1}. To check the pH sensitivity of Clensor's chloride response, fluorescence spectra were recorded for Clensor (200 nM) in 1× modified Cl^--clamping buffer (buffer Cl^- replaced with NO_3^-), pH 5, containing different added [Cl^-] ranging from 5 mM to 200 mM. The plot of normalized R/G as a function of [Cl^-], at pH 5, varies linearly with Cl^- from 0–200 mM with negligible change in Cl^- sensitivity compared to pH 7.4 (Supplementary Fig. 2). Furthermore, K_{SV} values obtained from the calibration profile of Clensor as a function of pH reveal that the Cl^- sensitivity of Clensor is pH-independent from pH 5 to 7.4 (Fig. 1e). This leaves Clensor well positioned to quantitate resting [Cl^-]$_{lumen}$ in the background of changing lumenal pH.

Clensor enables first measurement of lysosomal [Cl^-]

We next proceeded to quantitate [Cl^-] within specific endolysosomal compartments, including early endosomes (EEs), late endosomes (LEs), lysosomes (LYs) and recycling endosomes (REs). To target Clensor within specific endocytic compartments along the ALBR[23] and the transferrin receptor pathways[24], we used two molecular programming strategies. We have previously shown that DNA nanodevices are endocytosed in *Drosophila* haemocytes through the ALBR pathway and can map pH along the endolysosomal pathway[16,25]. We therefore chose *Drosophila* haemocytes to evaluate the intracellular performance of Clensor. Competition experiments with excess maleylated BSA (mBSA) confirmed that Clensor is internalized via this pathway (Fig. 2a). The residence times of internalized Clensor were determined in compartments along this pathway, namely EEs, LEs and LYs. *Drosophila* haemocytes expressing fluorescent fusions of molecular markers such as YFP-Rab5 for EEs, YFP-Rab7 for LEs/LYs and GFP-LAMP for

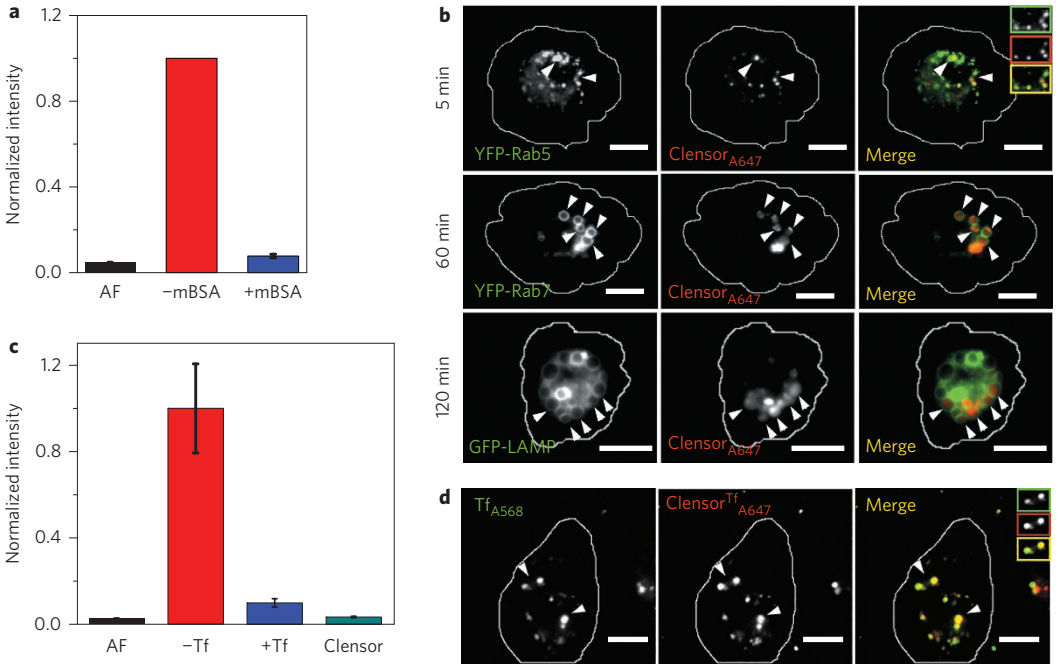

Figure 2 | Programming Clensor delivery to specific endocytic organelles. a, $Clensor_{A647}$ internalization by haemocytes in the presence (+mBSA) and absence (−mBSA) of excess competitor ligand maleylated BSA (mBSA, 10 μM) and autofluorescence (AF) in *Drosophila* haemocytes. Error bars indicate the mean of three independent experiments ± s.e.m. ($n = 20$ cells). **b**, Trafficking of Clensor ($Clensor_{A647}$) in haemocytes isolated from flies expressing YFP-Rab5 (upper row), YFP-Rab7 (middle row) and GFP-LAMP (lower row) at the indicated chase times. $Clensor_{A647}$-positive vesicles are shown in red and YFP-Rab5/YFP-Rab7/GFP-LAMP vesicles are shown in green. Scale bars, 10 μm. **c**, Competition experiments with $Clensor^{Tf}_{A647}$ and excess unlabelled transferrin (Tf, 25 μM). Normalized intensities of cells pulsed with $Clensor^{Tf}_{A647}$ in the presence (+Tf) and absence (−Tf) of Tf and $Clensor_{A647}$ are shown. Error bars indicate the mean of three independent experiments ± s.e.m. ($n = 15$ cells). **d**, Co-localization of $Clensor^{Tf}_{A647}$ with transferrin (Tf_{A568}) in S2R+ cells. Scale bars, 10 μm.

LYs[26] were labelled with a Clensor scaffold carrying only A647 ($Clensor_{A647}$). Time-dependent co-localization revealed that in *Drosophila* haemocytes, Clensor is resident predominantly in the EEs, LEs and LYs at 5 min, 60 min and 120 min, respectively (Supplementary Fig. 8). Figure 2b shows representative co-localization images in haemocytes between the indicated fluorescent compartment marker and $Clensor_{A647}$ at the indicated chase times, which are consistent with previous studies[16].

To quantify $[Cl^-]$ in REs ($[Cl^-]_{RE}$) using $Clensor^{Tf}$, we exploited the transferrin pathway in *Drosophila* S2R+ cells stably expressing the human transferrin (Tf) receptor[27]. When co-pulsing S2R+ cells with $Clensor^{Tf}$ carrying only A647 ($Clensor^{Tf}_{A647}$) and excess transferrin (+Tf), uptake of $Clensor^{Tf}_{A647}$ was efficiently abolished, confirming internalization via the transferrin receptor (Fig. 2c). Notably $Clensor_{A647}$ was not endocytosed by S2R+ cells, indicating that uptake was due to the transferrin aptamer engaging the transferrin receptor (Fig. 2c). Co-localization experiments with a mixture of Alexa 568 labelled transferrin (Tf_{A568}) and $Clensor^{Tf}_{A647}$ showed significant co-localization (~80%), revealing that $Clensor^{Tf}_{A647}$ predominantly resides in the REs 15 min post-endocytosis (Fig. 2d).

To check the intracellular functionality of Clensor, a standard Cl^- calibration profile was generated by clamping the $[Cl^-]_{lumen}$ to that of an externally added buffer containing known $[Cl^-]$ and a mixture of nigericin, valinomycin and tributyltin chloride (TBT-Cl) at high $[K^+]$[28]. Post endocytosis of Clensor, haemocytes were incubated in the clamping buffer for 1 h at room temperature and then imaged. The representative bitmap images presented in Fig. 3a indicate that cells clamped at different $[Cl^-]$ show distinct R/G maps. Figure 3b shows a histogram of R/G ratios obtained from populations of endosomes clamped at 5 mM, 40 mM and 80 mM $[Cl^-]$. Endosomal R/G ratios showed a linear dependence on $[Cl^-]$, with an ~2.5-fold change in R/G values from 5 mM to 120 mM $[Cl^-]$ (Fig. 3c,d, red). A standard Cl^- calibration profile for $Clensor^{Tf}$ in S2R+ cells also recapitulated these characteristics (Supplementary Fig. 10d). The intracellular and *in vitro* standard R/G profiles showed excellent correspondence, indicating that, post internalization, both Clensor and $Clensor^{Tf}$ recapitulate *in vitro* sensing properties quantitatively within cells. The intracellular R/G versus $[Cl^-]$ calibration profile is used for all subsequent determinations of endosomal chloride under physiological conditions.

Spatiotemporal $[Cl^-]$ changes were acquired in organelles along the ALBR pathway in haemocytes isolated from wild-type *D. melanogaster* (CS) larvae. Compartments along this pathway progressively acidify, yielding a pH ranging from ~6.0 in EEs to nearly ~5.0 in LYs[16]. Consistent with Cl^- being the dominant counterion for H^+ entry, the concentration of $[Cl^-]_{lumen}$ also increases along the endocytic pathway[8]. However, $[Cl^-]_{lumen}$ in lysosomes ($[Cl^-]_{LY}$) has not been reported thus far due to the lack of a suitable sensor[3]. In haemocytes, $[Cl^-]$ measurements were taken at chase times of 5, 60 and 120 min, corresponding to its residence in the EEs, LEs and LYs, respectively. Representative pseudocolour images of the haemocytes indicate the progressive accumulation of Cl^- (Fig. 4a). Histograms showing the spread of R/G ratios were obtained from a population of endosomes in each organelle, as indicated in Fig. 4b. The distribution of R/G ratios revealed a distinct shift to higher values, corresponding to an increase in $[Cl^-]_{lumen}$ during maturation along the endosomal/lysosomal pathway, where the mean $[Cl^-]_{EE}$ and $[Cl^-]_{LE}$ of 37.0 ± 1.6 mM and 60.4 ± 2 mM, respectively, are consistent with previous studies (Supplementary Table 3)[8,13]. Similarly, $Clensor^{Tf}$ reported a mean $[Cl^-]_{RE}$ of 39.9 ± 1.2 mM, consistent with the literature (Table 1)[13]. Overall, this indicates that Clensor can reliably measure $[Cl^-]$ in subcellular compartments. Given that Clensor functionality is unaffected at lysosomal pH, we measured $[Cl^-]_{LY}$. Quantification of the mean R/G values obtained from a population of lysosomes

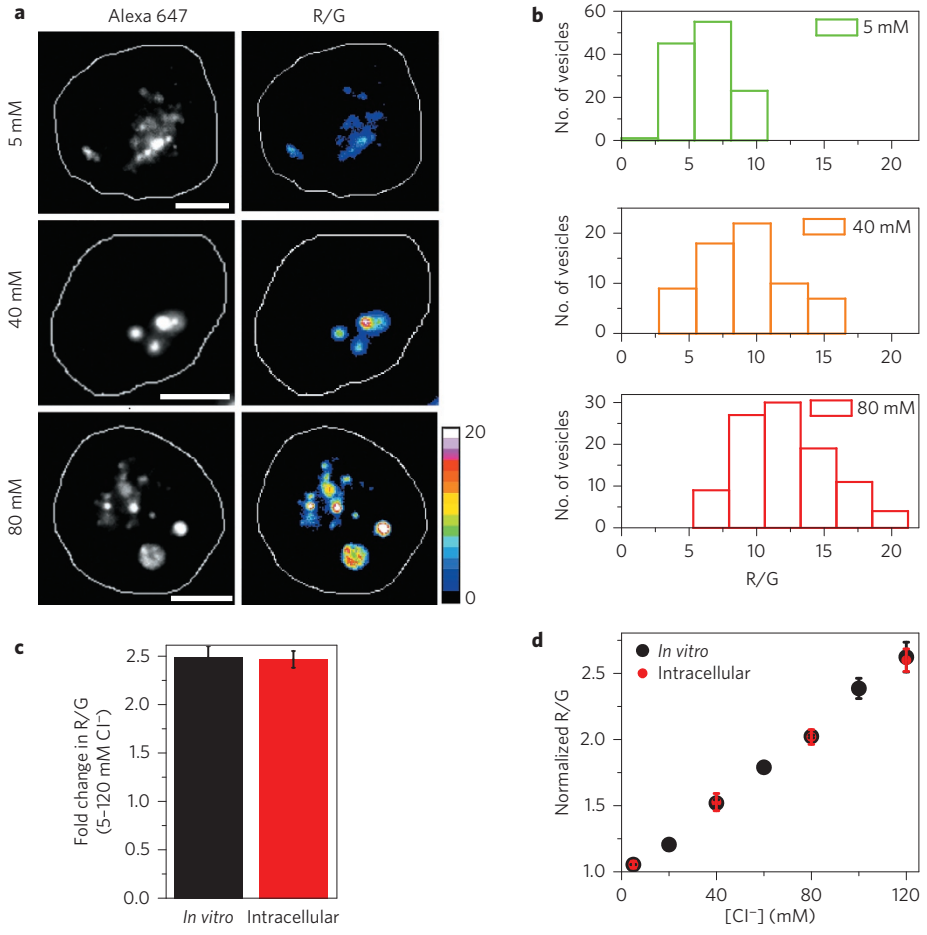

Figure 3 | Quantitative performance of Clensor within subcellular organelles. a, Alexa 647 channel and respective pseudocolour R/G map of *Drosophila* haemocytes pulsed with Clensor and clamped at 5, 40 and 80 mM Cl^-. Scale bars, 10 μm. **b**, Histograms showing typical spread of R/G ratios of vesicles clamped at 5, 40 and 80 mM Cl^- ($n \approx 10$ cells, ≥50 endosomes). **c**, *In vitro* and intracellular fold change in R/G ratios of Clensor at 5 and 120 mM Cl^-. **d**, Normalized R/G intensity (Alexa 647/BAC) ratios inside the endosomes, plotted as a function of $[Cl^-]$, yield the intracellular calibration profile (red), which is overlaid on the *in vitro* chloride calibration profile (black). Error bars indicate the mean of three independent experiments ± s.e.m. ($n \approx 10$ cells, ≥50 endosomes).

revealed a mean $[Cl^-]_{LY}$ of 108.5 ± 1.4 mM (Supplementary Table 3). To our knowledge, this is the first measurement of $[Cl^-]_{LY}$ and is also consistent with a theoretically computed of lysosomal $[Cl^-]$[29].

Localization and activity of DmClC-b and DmClC-c

Given that Clensor can reliably map absolute $[Cl^-]$ in specific endo-lysosomal compartments, as well as differences in $[Cl^-]$ in these compartments when Cl^- conductance is chemically perturbed (Supplementary Table 4), we used it to pinpoint the localization and activity of the putative intracellular CLC family proteins, DmClC-b and DmClC-c, in *Drosophila* (Supplementary Fig. 12). We investigated the function of DmClC-b and DmClC-c by genetically perturbing each of these genes and specifically measuring differences in $[Cl^-]$ in EEs, LEs, LYs and REs. DmClC-b and DmClC-c were specifically and efficiently knocked down in S2R+ cells by RNAi (Fig. 5a,b and Supplementary Fig. 13). $[Cl^-]_{RE}$ was measured in DmClC-c and DmClC-b knockdown S2R+ cells using $Clensor^{Tf}$. When DmClC-c was knocked down in S2R+ cells, $Clensor^{Tf}$ clearly revealed a modest reduction in Cl^- accumulation in these compartments, from 39.9 ± 1.2 mM to 33.1 ± 1.5 mM, indicating its high sensitivity (Table 1). Interestingly, $[Cl^-]_{RE}$ in DmClC-b RNAi cells remained unaltered (Table 1) indicating that DmClC-c is responsible for Cl^- accumulation in REs. To study the impact of Cl^- accumulation within REs on endosomal acidification, we carried out pH measurements in these compartments using fluorescein isothiocyanate (FITC) conjugated to transferrin (Tf-FITC) [25]. Table 1 shows a negligible increase in pH_{RE} (6.4 ± 0.03) in DmClC-c RNAi cells compared to untreated (6.3 ± 0.09) and DmClC-b RNAi (6.3 ± 0.09) cells.

To understand the role of DmClC-b and DmClC-c at each stage of endolysosomal maturation, we used UAS-RNAi-based depletion of DmClC-b and DmClC-c in *Drosophila* larvae and measured Cl^- accumulation using Clensor within EEs, LEs and LYs along the ALBR pathway in haemocytes from these larvae. Analysis by polymerase chain reaction with reverse transcription (RT-PCR) showed significant and specific reduction of the DmClC-b and DmClC-c transcripts (Fig. 4c,d). In EEs of DmClC-c RNAi haemocytes, Cl^- accumulation was significantly decreased to 28.9 ± 0.8 mM compared to 37.0 ± 1.6 mM in CS (Fig. 4e, Supplementary Fig. 11a and Table 3). However, Cl^- accumulation in LEs and LYs remained unaltered (Fig. 4f,g, Supplementary Fig. 11b,c and Supplementary Table 3). Notably, $[Cl^-]_{EE}$ in haemocytes depleted of DmClC-b remained unaltered (Fig. 4e, Supplementary Fig. 11a and Supplementary Table 3), indicating that DmClC-c predominantly facilitates Cl^- accumulation in EEs and REs.

To study the effect of Cl^- accumulation on pH_{EE}, haemocytes were co-pulsed with FITC dextran (FD10) and $Clensor_{A647}$ to mark EEs of the ALBR pathway. Compartmental pH was obtained from $\lambda_{Ex} = 480/\lambda_{Ex} = 430$ intensity ratios from only those endosomes containing FD10 as well as $Clensor_{A647}$ (Fig. 4h and

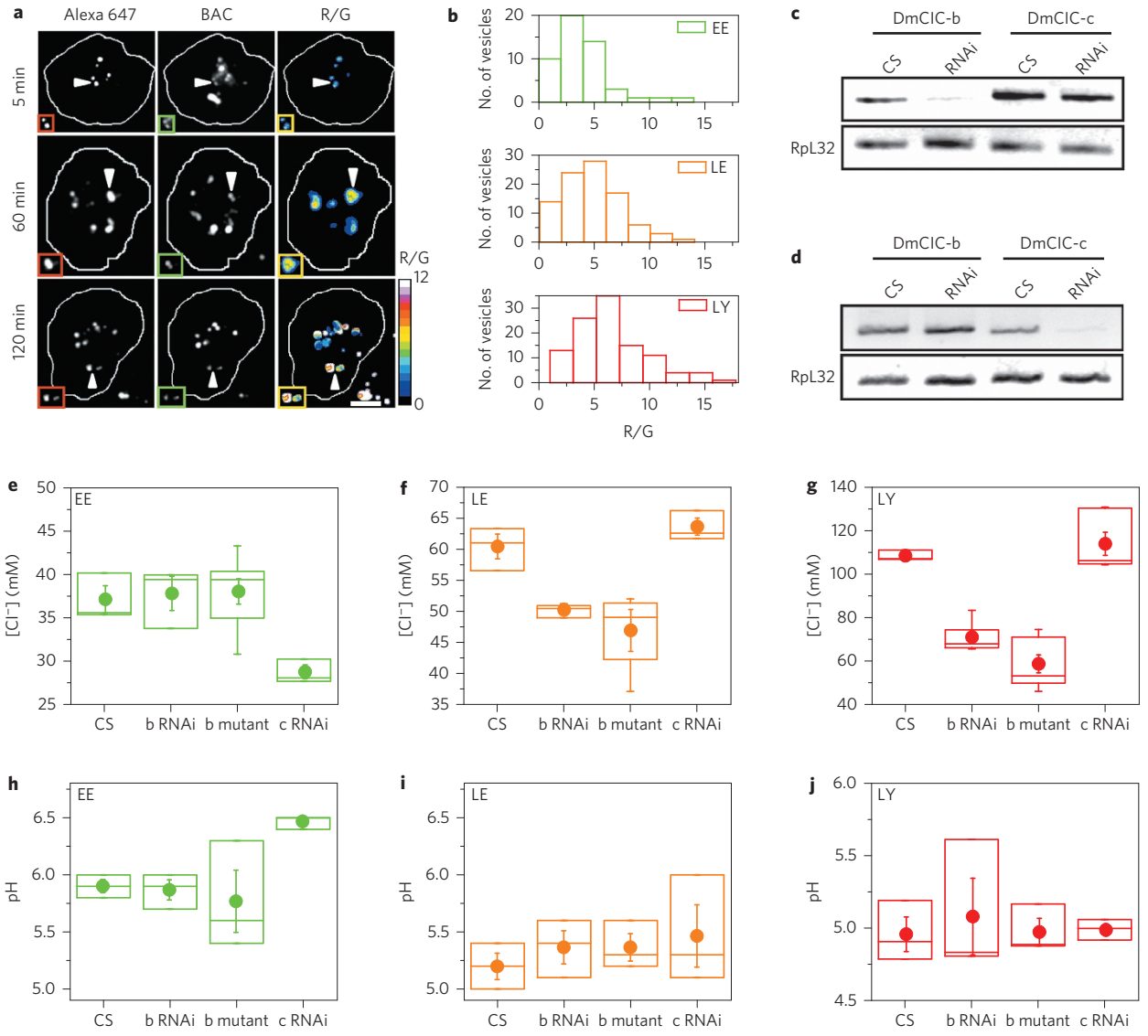

Figure 4 | Spatiotemporal mapping of [Cl⁻] along the endolysosomal pathway using Clensor in living cells. a, Representative pseudocolour R/G map of live haemocytes isolated from wild-type *Drosophila* and labelled with Clensor. Scale bar, 10 μm. **b**, Histograms of R/G ratios of EE at 5 min (green), LE at 60 min (orange) and LY at 120 min (red) ($n \approx 20$ cells, ~100 endosomes/lysosomes). **c**,**d**, RT-PCR analysis of total RNA isolated from 3rd instar larvae of UAS-DmClC-b RNAi/Coll GAL4 larvae (DmClC-b RNAi) (**c**) and UAS-DmClC-c RNAi/Coll GAL4 larvae (DmClC-c RNAi) (**d**). Lanes marked as CS correspond to PCR-amplified cDNA of the indicated gene products (DmClC-b and DmClC-c) from wild-type *Drosophila*, and lanes marked as RNAi are for the corresponding gene products isolated from 3rd instar larvae of UASDmClC-b RNAi/Coll GAL4 (**c**) and UAS-DmClC-c RNAi/CollGAL4 (**d**) flies. RpL32 was used as a loading control. **e**–**g**, Box plots showing [Cl⁻] distributions for EE (**e**), LE (**f**) and LY (**g**) in haemocytes of the indicated genetic background ($n \sim 15$ cells, ~75 endosomes/lysosomes). **h**,**i**, Box plots showing pH distributions in EE (**h**) and LE (**i**) in haemocytes of the indicated genetic background using the FD10 dual excitation method. **j**, Box plots showing pH distribution in LY in haemocytes of the indicated genetic background using I4LY A488/A647 ($n > 15$ cells, >50 endosomes/lysosomes. In **e**–**j**: CS, wild-type; b RNAi, RNAi against DmClC-b; b mutant, DmClC-b mutant; c RNAi, DmClC-c RNAi. Boxes represent 25–75% of the population. Horizontal lines within boxes represent the median. Filled circles represent mean of the data obtained for each indicated genotype. Error bars on filled circles represent s.e.m.

Supplementary Table 3). We observed that the lumen of EEs depleted of DmClC-c showed drastic hypo-acidification, with a mean pH of 6.4 ± 0.03 compared to 5.9 ± 0.06 in CS (Supplementary Table 3). Importantly, pH_{LE} and pH_{LY} in these haemocytes were unaffected (Fig. 4i,j and Supplementary Table 3), indicating that Cl^- accumulation due to DmClC-c largely facilitates acidification of EEs.

We also investigated the role of DmClC-b along the same pathway. Interestingly, [Cl⁻] measurements using Clensor in DmClC-b RNAi haemocytes revealed impaired Cl^- accumulation in both LEs and LYs (Fig. 4f,g, Supplementary Fig. 11b,c and Supplementary Table 3). $[Cl^-]_{LE}$ reduced to 50.1 ± 0.5 mM from 60.4 ± 2 mM in CS and $[Cl^-]_{LY}$ decreased to 70.9 ± 2.8 mM from 108.5 ± 1.4 mM in CS (Supplementary Table 3). We reaffirmed this in haemocytes from a transgenic fly line, DmClC-b mutant, where DmClC-b is disrupted due to p-element insertion (Supplementary Table 6). Cl^- measurements in these haemocytes using Clensor showed severe Cl^- accumulation defects within LEs and LYs (Supplementary Figs 11b,c and 14d). The role of DmClC-b in compartment acidification was assessed by measuring pH_{LE} using FD10 as described earlier and pH_{LY} using a modified I-switch ($I4^{LY}_{A488/A647}$), in both DmClC-b RNAi and DmClC-b mutant haemocytes. Interestingly, these investigations revealed that pH_{LE} and pH_{LY} along the ALBR pathway remained unaltered

Table 1 | Lumenal $[Cl^-]_{RE}$ within recycling endosomes.

	Mean $[Cl^-]_{RE}$ ± s.e.m. (mM)	Mean pH_{RE} ± s.e.m.
S2R+	39.9 ± 1.2	6.3 ± 0.09
DmClC-c RNAi	33.1 ± 1.5	6.4 ± 0.03
DmClC-b RNAi	39.1 ± 0.7	6.3 ± 0.09

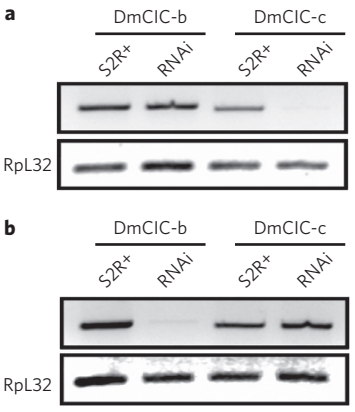

Figure 5 | Clensor^{Tf} maps $[Cl^-]$ within recycling endosomes (REs). **a**,**b**, RNAi knockdown of DmClC-c and DmClC-b in *Drosophila* S2R+ cells. PCR-amplified cDNA of the indicated gene products (DmClC-b and DmClC-c) isolated from untreated and RNAi treated *Drosophila* S2R+ cells for RNAi against DmClC-c (**a**) and RNAi against DmClC-b (**b**). RpL32 was used as loading control.

compared to CS, despite such drastic impairment of Cl^- accumulation (Fig. 4i,j, Supplementary Table 3 and Supplementary Fig. 14d). This indicates that DmClC-b predominantly facilitates Cl^- accumulation in LEs and LYs, without impacting acidification in these compartments. The localization of DmClC-b in the LE/LY and DmClC-c in in the EE/RE of the *Drosophila* cells was confirmed by co-immunofluorescence in S2R+ cells (Supplementary Fig. 16).

Conclusions

The modularity of the DNA scaffold allows one to molecularly program a single nanodevice with a sensing module, a normalizing module and a targeting module. By integrating aptamer modules to Clensor one can obtain nanodevices with identical sensor characteristics that are localizable within a desired subcellular compartment. This essentially makes Clensor a plug-and-play tool for diverse endocytic pathways, where one does not need to chemically fabricate a new sensor, and assays across different systems may therefore be compared.

The accuracy and pH-independent nature of Clensor in measuring resting organellar chloride enables quantification of the activity of endogeneous intracellular chloride transporters. Among the three CLC family channels and transporters in *D. melanogaster*, the putative intracellular CLC family proteins DmClC-b and DmClC-c were unexplored. DmClC-c shows sequence homology with the second branch of mammalian CLC transporters (ClC-3, 4, 5). Members of this branch are known to localize in EEs, REs and LEs and facilitate Cl^- accumulation[30,31] and impact endosomal acidification therein[32]. Clensor revealed that DmClC-c is resident primarily in EEs and REs, where it effects chloride accumulation, which is coupled to lumenal acidification in the EE. DmClC-b shares sequence homology with ClC-6 and ClC-7 in mammals. ClC-6 resides predominantly in LEs of neurons[33], and the ubiquitously expressed ClC-7 localizes in LEs/LYs[34]. Interestingly, ClC-7 and ClC-6 knockout mice also show unaltered lysosomal pH due to compensatory cation conductance in these organelles[35,36]. Despite a relative quantification of $[Cl^-]_{LY}$, an absolute measure of lysosomal chloride (which would help delineate the role of ClC-6 and ClC-7 in lysosomal chloride homeostasis[29]) had remained elusive. However, by targeting Clensor along the ALBR pathway in *Drosophila* haemocytes, we have been able to report $[Cl^-]_{LY}$ for the first time. Notably, Clensor also revealed that DmClC-b mainly facilitates Cl^- accumulation in the LYs, without affecting acidification in these compartments. This indicates a role for $[Cl^-]_{lumen}$ in lysosomes and its molecular connections to physiology, especially in various lysosomal storage disorders. For example, mice deficient in ClC-7[37] or carrying 'uncoupled' ClC-7[29] show no change in lysosomal pH, yet manifest lysosomal disorders, neurodegeneration and osteopetrosis, suggesting far-reaching functions of lysosomal Cl^- beyond pH regulation[38]. The cellular activity of many putative intracellular Cl^- transport proteins[3] such as the cystic fibrosis transmembrane conductance regulator (CFTR) and Golgi pH regulator (GPHR) in physiology and disease could be assayed by directly measuring $[Cl^-]$ in live cells. Furthermore, the role of chloride in pH homeostasis along the secretory pathway[39] as well as in synaptic vesicles remains under-explored[2,3]. Combined with suitable targeting strategies, the pH-independent chloride sensing property of Clensor could provide new insights into chloride biology[3].

Methods

Methods and any associated references are available in the online version of the paper.

Received 2 August 2014; accepted 22 May 2015; published online 22 June 2015

References

1. Sheppard, D. N. & Welsh, M. J. Structure and function of the CFTR chloride channel. *Physiol. Rev.* **79,** S23–S45 (1999).
2. Stauber, T., Weinert, S. & Jentsch, T. J. Cell biology and physiology of CLC chloride channels and transporters. *Compr. Physiol.* **2,** 1701–1744 (2012).
3. Stauber, T. & Jentsch, T. J. Chloride in vesicular trafficking and function. *Annu. Rev. Physiol.* **75,** 453–477 (2013).
4. Kuner, T. & Augustine, G. J. A genetically encoded ratiometric indicator for chloride: capturing chloride transients in cultured hippocampal neurons. *Neuron* **27,** 447–459 (2000).
5. Markova, O., Mukhtarov, M., Real, E., Jacob, Y. & Bregestovski, P. Genetically encoded chloride indicator with improved sensitivity. *J. Neurosci. Methods* **170,** 67–76 (2008).
6. Arosio, D. *et al.* Simultaneous intracellular chloride and pH measurements using a GFP-based sensor. *Nature Methods* **7,** 516–518 (2010).
7. Casey, J. R., Grinstein, S. & Orlowski, J. Sensors and regulators of intracellular pH. *Nature Rev. Mol. Cell Biol.* **11,** 50–61 (2010).
8. Sonawane, N. D., Thiagarajah, J. R. & Verkman, A. S. Chloride concentration in endosomes measured using a ratioable fluorescent Cl^- indicator: evidence for chloride accumulation during acidification. *J. Biol. Chem.* **277,** 5506–5513 (2002).
9. Krapf, R., Illsley, N. P., Tseng, H. C. & Verkman, A. S. Structure–activity relationships of chloride-sensitive fluorescent indicators for biological application. *Anal. Biochem.* **169,** 142–150 (1988).
10. Verkman, A. S. Development and biological applications of chloride-sensitive fluorescent indicators. *Am. J. Physiol.* **259,** C375–C388 (1990).
11. Biwersi, J., Tulk, B. & Verkman, A. S. Long-wavelength chloride-sensitive fluorescent indicators. *Anal. Biochem.* **219,** 139–143 (1994).
12. Geddes, C. D. Optical halide sensing using fluorescence quenching: theory, simulations and applications—a review. *Meas. Sci. Technol.* **12,** R53 (2001).
13. Sonawane, N. D. & Verkman, A. S. Determinants of $[Cl^-]$ in recycling and late endosomes and Golgi complex measured using fluorescent ligands. *J. Cell Biol.* **160,** 1129–1138 (2003).
14. Bhatia, D., Sharma, S. & Krishnan, Y. Synthetic, biofunctional nucleic acid-based molecular devices. *Curr. Opin. Biotechnol.* **22,** 475–484 (2011).
15. Krishnan, Y. & Bathe, M. Designer nucleic acids to probe and program the cell. *Trends Cell Biol.* **22,** 624–633 (2012).
16. Modi, S. *et al.* A DNA nanomachine that maps spatial and temporal pH changes inside living cells. *Nature Nanotech.* **4,** 325–330 (2009).
17. Modi, S., Nizak, C., Surana, S., Halder, S. & Krishnan, Y. Two DNA nanomachines map pH changes along intersecting endocytic pathways inside the same cell. *Nature Nanotech.* **8,** 459–467 (2013).

18. Bhatia, D. *et al.* Icosahedral DNA nanocapsules by modular assembly. *Angew. Chem. Int. Ed.* **48,** 4134–4137 (2009).
19. Lee, H. *et al.* Molecularly self-assembled nucleic acid nanoparticles for targeted *in vivo* siRNA delivery. *Nature Nanotech.* **7,** 389–393 (2012).
20. Surana, S., Bhat, J. M., Koushika, S. P. & Krishnan, Y. An autonomous DNA nanomachine maps spatiotemporal pH changes in a multicellular living organism. *Nature Commun.* **2,** 340 (2011).
21. Modi, S., Halder, S., Nizak, C. & Krishnan, Y. Recombinant antibody mediated delivery of organelle-specific DNA pH sensors along endocytic pathways. *Nanoscale* **6,** 1144–1152 (2014).
22. Wilner, S. E. *et al.* An RNA alternative to human transferrin: a new tool for targeting human cells. *Mol. Ther. Nucleic Acids* **1,** e21 (2012).
23. Guha, A., Sriram, V., Krishnan, K. S. & Mayor, S. *Shibire* mutations reveal distinct dynamin-independent and -dependent endocytic pathways in primary cultures of *Drosophila* hemocytes. *J. Cell Sci.* **116,** 3373–3386 (2003).
24. Mayle, K. M., Le, A. M. & Kamei, D. T. The intracellular trafficking pathway of transferrin. *Biochim. Biophys. Acta* **1820,** 264–281 (2012).
25. Bhatia, D., Surana, S., Chakraborty, S., Koushika, S. P. & Krishnan, Y. A synthetic icosahedral DNA-based host–cargo complex for functional *in vivo* imaging. *Nature Commun.* **2,** 339 (2011).
26. Huotari, J. & Helenius, A. Endosome maturation. *EMBO J.* **30,** 3481–3500 (2011).
27. Gupta, G. D. *et al.* Analysis of endocytic pathways in *Drosophila* cells reveals a conserved role for GBF1 in internalization via GEECs. *PLoS ONE* **4,** e6768 (2009).
28. Krapf, R., Berry, C. A. & Verkman, A. S. Estimation of intracellular chloride activity in isolated perfused rabbit proximal convoluted tubules using a fluorescent indicator. *Biophys J.* **53,** 955–962 (1988).
29. Weinert, S. *et al.* Lysosomal pathology and osteopetrosis upon loss of H^+-driven lysosomal Cl^- accumulation. *Science* **328,** 1401–1403 (2010).
30. Hara-Chikuma, M. *et al.* ClC-3 chloride channels facilitate endosomal acidification and chloride accumulation. *J. Biol. Chem.* **280,** 1241–1247 (2005).
31. Hara-Chikuma, M., Wang, Y., Guggino, S. E., Guggino, W. B. & Verkman, A. S. Impaired acidification in early endosomes of ClC-5 deficient proximal tubule. Biochem. *Biochem. Biophys. Res. Commun.* **329,** 941–946 (2005).
32. Mohammad-Panah, R. *et al.* An essential role for ClC-4 in transferrin receptor function revealed in studies of fibroblasts derived from Clcn4-null mice. *J. Cell Sci.* **122,** 1229–1237 (2009).
33. Poët, M. *et al.* Lysosomal storage disease upon disruption of the neuronal chloride transport protein ClC-6. *Proc. Natl Acad. Sci. USA* **103,** 13854–13859 (2006).
34. Kasper, D. *et al.* Loss of the chloride channel ClC-7 leads to lysosomal storage disease and neurodegeneration. *EMBO J.* **24,** 1079–1091 (2005).
35. Mindell, J. A. Lysosomal acidification mechanisms. *Annu. Rev. Physiol.* **74,** 69–86 (2012).
36. DiCiccio, J. E. & Steinberg, B. E. Lysosomal pH and analysis of the counter ion pathways that support acidification. *J. Gen. Physiol.* **137,** 385–390 (2011).
37. Kornak, U. *et al.* Loss of the ClC-7 chloride channel leads to osteopetrosis in mice and man. *Cell* **104,** 205–215 (2001).
38. Scott, C. C. & Gruenberg, J. Ion flux and the function of endosomes and lysosomes: pH is just the start. *BioEssays* **33,** 103–110 (2011).
39. Weisz, O. A. Acidification and protein traffic. *Int. Rev. Cytol.* **226,** 259–319 (2003).

Acknowledgements

The authors thank the Central Imaging and Flow Facility at the National Centre for Biological Sciences (NCBS) for imaging. This work was funded by the Wellcome Trust Department of Biotechnology (DBT), the India Alliance and the University of Chicago. S.S., S.H. and V.P. acknowledge the Council of Scientific and Industrial Research (CSIR), Government of India, for fellowship. FLIM experiments were performed at the Northwestern University Center for Advanced Microscopy supported by NCI CCSG P30 CA060553 awarded to the Robert H. Lurie Comprehensive Cancer Center.

Author contributions

S.S., K.C., V.P. and Y.K. conceived and designed the experiments. S.S., V.P. and K.C. performed the experiments. S.H. designed the $I4^{LY}_{A488/A647}$ used herein. S.S., V.P., K.C. and Y.K. analysed the data. S.S. and Y.K. co-wrote the paper. All authors commented on the manuscript.

Additional information

Supplementary information is available in the online version of the paper. Reprints and permissions information is available online at www.nature.com/reprints. Correspondence and requests for materials should be addressed to Y.K.

Competing financial interests

The authors declare no competing financial interests.

Methods

Fly stocks and cell culture. All fly stocks were obtained from Bloomington Stock Centre at Indiana University, unless otherwise indicated (Supplementary Table 6), and were maintained as described earlier[40]. Haemocytes were obtained from *Drosophila* 3rd instar larvae as described previously[40]. S2R+ cells were a gift from Satyajit Mayor's laboratory[27] and were maintained as described previously[27].

Sample preparation. High-performance liquid chromatography (HPLC) purified and lyophilized oligonucleotides (IBA GmbH) and PNA oligomer were dissolved in Milli-Q water (Millipore), aliquoted and stored at −20 °C until further use. Stock solutions of Clensor were prepared at a final concentration of 10 μM by mixing D1, D2 and P in an equimolar ratio in 10 mM sodium phosphate buffer, pH 7.4. For Clensor^{Tf} samples, D1Tf$_{apt}$, D2 and P were mixed in equimolar ratios at a final concentration of 10 μM in 10 mM sodium phosphate buffer, pH 7.4, containing 1 mM EDTA, pH 8. For $I4^{LY}_{A488/A647}$ sample preparation, 5 μM of I4 and I4′ were mixed in equimolar ratios in 20 mM potassium phosphate buffer, pH 5.5, containing 100 mM KCl. Annealing was performed by heating the solution at 90 °C for 5 min and cooling at a rate of 5 °C/15 min.

Steady-state fluorescence measurements. All fluorescence studies were carried out on a Fluoromax-4 (Horiba Scientific) spectrophotometer. A 10 μM stock of Clensor was diluted to a final concentration of 200 nM using 10 mM sodium phosphate buffer, pH 7.4 or 1× modified pH clamping buffer with pH ranging from 5 to 7, and incubated for 30 min at room temperature before experiments. The emission spectra of BAC and A647 were acquired by exciting the samples at 435 nm (λ^{BAC}_{Ex}) and 650 nm (λ^{A647}_{Ex}), respectively. Emission spectra of BAC and A647 were collected between 495 and 550 nm and 650 and 700 nm, respectively. To study the chloride sensitivity of Clensor, final values of [Cl^-] ranging between 5 mM to 200 mM were achieved by adding microlitre aliquots of a 1 M stock of NaCl to the samples. The emission intensity of BAC at 505 nm (G) was normalized to the emission intensity of A647 at 670 nm (R). The fold change in R/G ratio was calculated from the ratio of R/G values at two specific values of [Cl^-].

Co-localization assays. Transgenic flies expressing UAS-YFP.Rab5 (Bloomington Drosophila Stock Center at Indiana University), UAS-YFP.Rab7 (Bloomington Drosophila Stock Center at Indiana University) and UAS-GFP.LAMP[1] were crossed with flies expressing haemocytes-specific driver Collagen-GAL4. All crosses were maintained at 25 °C. Haemocytes from larvae obtained from these crosses were isolated and pulsed with 1 μM Clensor$_{A647}$ (Clensor scaffold carrying only Alexa 647) for 5 min, followed by chase periods of 5, 60 and 120 min, as specified, at 20 °C. The cells were then washed with 1× M1 buffer and imaged.

S2R+ cells were labelled with a mixture of 1 μM $Clensor^{Tf}_{A647}$ (Clensor^{Tf} scaffold carrying only Alexa 647) and 100 nM Tf$_{A568}$, as described earlier.

Chloride clamping of cells. Haemocytes and S2R+ cells were pulsed with 2 μM Clensor and Clensor^{Tf}, respectively. Haemocytes were then fixed with paraformaldehyde (2.5% PFA) for 2 min at room temperature and clamped at the desired [Cl^-] by incubation in appropriate chloride clamping buffer containing 10 μM nigericin, 10 μM valinomycin and 10 μM TBT-Cl for 1 h at room temperature.

Cells were fixed with 2.5% PFA for 20 min at room temperature and clamped at the desired [Cl^-] by incubation in appropriate chloride clamping buffer containing 10 μM nigericin, 10 μM valinomycin, 5 μM carbonyl cyanide-m-chlorophenylhydrazone, 10 μM monensin and 200 nM bafilomycin for 3 h at room temperature.

Chloride measurements. For chloride measurements, haemocytes were pulsed with 2 μM Clensor and then chased for (1) 5 min (EE), (2) 60 min (LE) and (3) 120 min (LY). Each set of cells was then imaged in BAC as well as A647 channels for each field of view, as described in the image analysis section. To measure chloride concentrations in REs, S2R+ cells were pulsed with Clensor^{Tf}, chased for 15 min and then imaged.

RNAi in S2R+ cells. Depletions were performed as described previously[41].

pH clamping and measurement. For the intracellular pH calibration curve, haemocytes and S2R+ cells were labelled with FD10 (2 mg ml^{-1})/$I4^{LY}_{A488/A647}$ (1 μM) and Tf-FITC (100 nM), respectively. The cells were then clamped at the desired pH as described earlier[16]. pH_{EE}, pH_{LE} and pH_{RE} measurements using FD10/ Tf-FITC were performed as described earlier[25]. pH_{LY} measurements using $I4^{LY}_{A488/A647}$ were performed as described earlier[16].

Fluorescence microscope set-up. For chloride measurements, cells were imaged on an Olympus IX81 (Olympus) inverted microscope equipped with a mercury halide lamp (Olympus) and a 512 × 512, iXon^{EM}CCD camera (Andor) using Micro-Manager 1.4.7 software (The University of California, San Francisco). BAC channel images (referred to as 'G') were acquired using a 480/20 band pass excitation filter, a 535/40 band pass emission filter and an 86023bs-FITC/Cy5 as dichroic filter. A647 channel images (referred to as 'R') were obtained using a 640/30 band pass excitation filter, a 690/50 band pass emission filter and an HQ665lp-665 long pass dichroic filter.

For pH measurements, two sets of images were acquired by exciting the cells using 430/30 (λ_{Ex}430) and 480/30 (λ_{Ex}480) band pass excitation filters. In both cases, emissions were collected using a 535/40 band pass emission filter and an 89006bs-CFP/YFP/RFP dichroic filter. For pH measurements in haemocytes, one extra set of images was acquired in the A647 channel.

Image analysis. Images were analysed with ImageJver 1.47 (NIH).

References

40. Sriram, V., Krishnan, K. S. & Mayor, S. Deep-orange and carnation define distinct stages in late endosomal biogenesis in *Drosophila melanogaster*. *J. Cell Biol.* **161,** 593–607 (2003).
41. Clemens, J. C. *et al.* Use of double-stranded RNA interference in *Drosophila* cell lines to dissect signal transduction pathways. *Proc. Natl Acad. Sci. USA* **97,** 6499–6503 (2000).